

## Modeling multiband emissions from two young SNRs with a time-dependent magnetic field \*

Yun-Yong Tang<sup>1</sup>, Zu-Cheng Dai<sup>1</sup> and Li Zhang<sup>2</sup>

<sup>1</sup> Department of Physical Science and Technology, Kunming University, Kunming 650031, China; [tangyunyong888@163.com](mailto:tangyunyong888@163.com)

<sup>2</sup> Department of Physics, Yunnan University, Kunming 650091, China

Received 2012 September 3; accepted 2012 December 7

**Abstract** The nonthermal components in hard X-rays have been detected in two young supernova remnants (SNRs): SN 1006 and Kepler’s SNR. Various theoretical models showed that the amplification of the magnetic field was crucial to explain their multiband emission properties. We investigate the evolution of the magnetic field and model the multiband emissions from these two young SNRs with a time-dependent injection model. The results indicate that (1) the radio and X-ray emissions are reproduced by synchrotron radiation of the injected electrons, while the  $\gamma$ -rays can be explained as inverse Compton scattering of the relativistic electrons and proton-proton interaction of the high-energy protons; and (2) the amplification of the magnetic field spontaneously happens with reasonable parameters.

**Key words:** radiation mechanisms: non-thermal — gamma-rays: theory — (ISM:) supernova remnant

### 1 INTRODUCTION

The origin of Galactic cosmic rays is closely related to supernova remnants (SNRs), and young SNRs are no exception. SN 1006 (G327.6+14.6) and Kepler’s SNR (G4.5+6.8) are two of the most interesting SNRs in many areas of astrophysics. The nonthermal component of X-rays has been reported for SN 1006 (Koyama et al. 1995; Willingale et al. 1996; Bamba et al. 2003; Long et al. 2003; Rothenflug et al. 2004) and Kepler’s SNR (Becker et al. 1980; Cassam-Chenaï et al. 2004; Bamba et al. 2005). These observations strongly imply a synchrotron origin of the radiation from accelerated electrons, which can be accelerated up to highly relativistic energies (Koyama et al. 1995; Reynolds 1996). Historically, the diffusive shock acceleration is the most popular acceleration mechanism in SNRs (Bell 1978; Blandford & Ostriker 1978), and various models have been put forward to account for the multiband emission from young SNRs.

By using the known range of astronomical parameters and the existing measurements of non-thermal emission in SNR SN 1006, Berezhko et al. (2009) discussed the acceleration efficiency of cosmic rays, and thought that SN 1006 was a high-efficiency nuclear cosmic-ray factory, and the amplified magnetic field was strongly related to the hard X-ray morphology of the synchrotron emission. Recently, Petruk et al. (2011) presented a new way to compare models and observations.

---

\* Supported by the National Natural Science Foundation of China.

Based on classical magnetohydrodynamic and cosmic-ray acceleration theories, their model could be used to put observational constraints on the magnetic field and to survey the spatial distribution of SN 1006. The detection of very high energy (VHE)  $\gamma$ -rays from SN 1006 has been carried out by the HESS collaboration (Acero et al. 2010), who presented a simple phenomenological model, in which a single power-law spectral shape was assumed with an exponential cutoff. They modeled the multiband spectra of SN 1006, where obviously the magnetic field was an important physical parameter for different models. Similarly, Berezhko et al. (2007) found the multifrequency properties of Kepler's SNR by using the nonlinear kinetic theory of cosmic ray acceleration, and constrained the physical parameters of this SNR with a large magnetic field that is imposed on fitting the observations. In the meantime, they predicted the  $\gamma$ -ray spectrum expected from Kepler's SNR.

In this paper, we consider the temporal evolution of the magnetic field and recalculate the maximum energy of accelerated particles (electrons and protons). Then the temporally evolving non-thermal particle and photon spectra of two young SNRs are presented at different stages with the time-dependent model (Sturmer et al. 1997; Zhang & Fang 2007). In Section 2, we present some details of the model, including shock dynamics of SNRs, temporal evolution of the magnetic field, energy spectra of accelerated particles, particle energy distributions, and so on. The model is applied to two young SNRs and the results are shown in Section 3. Finally, we present our conclusions and discussion.

## 2 ANALYTIC MODEL

The temporal evolution of photon emission from SNRs has been modeled through a three step process (Zhang & Fang 2007). First of all, the acceleration mechanism of accelerated particles was considered in the diffusive shock acceleration. Subsequently, the temporal evolution of particle energy distributions was produced, and then those authors described the emission of photons. In this section, the shock dynamics of SNRs is reviewed. Moreover, we reconsider the maximum energy of accelerated particles, and the evolution of the magnetic field is investigated in terms of the lifetime of SNRs.

### 2.1 Evolution of SNRs

After the supernova explosion occurs, the ejected material with initial mass  $M_{\text{ej}}$  expands into the uniform ambient medium with density  $n_0$ , bounding the SNR by an expanding shock wave. Lozinskaya (1992) showed that SNRs evolve through three stages: the free expansion stage, the Sedov stage, and the radiative stage. The free expansion stage ends at  $t_{\text{Sed}} \approx 2.1 \times 10^2 (E_{51}/n_0)^{1/3} v_9^{5/3}$  yr, and the Sedov stage ends when  $t_{\text{rad}} \approx 4.0 \times 10^4 E_{51}^{4/17} n_0^{-9/17}$  yr.  $v_9$  mentioned above is the initial velocity ( $v_0$ ) in units of  $10^9 \text{ cm s}^{-1}$ . Ohira et al. (2012) showed simple evolutions of the shock radius  $R_{\text{sh}}$  and the shock velocity  $u_{\text{sh}}$  occur as follows:

$$R_{\text{sh}}(t) = v_0 t_{\text{Sed}} \times \begin{cases} \left(\frac{t}{t_{\text{Sed}}}\right) & (t \leq t_{\text{Sed}}) \\ \left(\frac{t}{t_{\text{Sed}}}\right)^{2/5} & (t_{\text{Sed}} \leq t) \end{cases}, \quad (1)$$

$$u_{\text{sh}}(t) = v_0 \times \begin{cases} 1 & (t \leq t_{\text{Sed}}) \\ \left(\frac{t}{t_{\text{Sed}}}\right)^{-3/5} & (t_{\text{Sed}} \leq t) \end{cases}. \quad (2)$$

In the diffusive shock acceleration mechanism, the acceleration time

$$t_{\text{acc}} = \eta_{\text{acc}} D / u_{\text{sh}}^2(t) = \eta_{\text{acc}} \eta_{\text{g}}(t) c E / (3eB(t)u_{\text{sh}}^2(t)),$$

where  $D$  is the diffusion coefficient around the shock, and  $E$  and  $B(t)$  are the energy of cosmic rays and the magnetic field in the upstream region, respectively.  $\eta_{\text{g}}(t)$  is the gyrofactor and  $\eta_{\text{acc}} \approx 10$  is

a numerical factor which depends on the shock compression ratio. With the condition  $t_{\text{acc}} = t$ , the maximum energy of accelerated particles, which is limited by their lifetime, is presented as

$$E_{\text{m,age}} = \frac{3eB(t)[R_{\text{sh}}(t_{\text{Sed}})]^2}{\eta_{\text{acc}}\eta_{\text{g}}(t)ct_{\text{Sed}}} \times \begin{cases} \left(\frac{t}{t_{\text{Sed}}}\right) & t \leq t_{\text{Sed}} \\ \left(\frac{t}{t_{\text{Sed}}}\right)^{-\frac{1}{5}} & t_{\text{Sed}} \leq t \end{cases} . \quad (3)$$

Moreover, the maximum value of the condition  $t_{\text{acc}} = t_{\text{esc}}$ , which is limited by the time for the particles to escape, is given as

$$E_{\text{m,esc}} = \sqrt{\eta_{\text{acc}}\eta_{\text{esc}}}E_{\text{m,age}} , \quad (4)$$

with  $\sqrt{\eta_{\text{acc}}\eta_{\text{esc}}} = 1$  for simplicity (Ohira et al. 2012). In the early stages, the particle's maximum energy is limited by the SNR's age. Then significant synchrotron cooling will confine the maximum energy of an electron, so the cooling time of electrons due to synchrotron emission can be expressed by  $t_{\text{cool,e}} = 9m_e^4c^7/(4e^4B_d^2(t)E)$ , where  $B_d(t)$  is the the magnetic field in the downstream region. The maximum energy, limited by cooling from the condition  $t_{\text{acc}} = t_{\text{cool,e}}$ , can be expressed as

$$E_{\text{m,cool}} = E_{\text{m,S}} \times \begin{cases} 1 & t \leq t_{\text{Sed}} \\ \left(\frac{t}{t_{\text{Sed}}}\right)^{\frac{2\alpha_{\text{B}}-\alpha-1}{2}} & t_{\text{Sed}} \leq t \leq t_{\text{B}} \\ \left(\frac{t_{\text{B}}}{t_{\text{Sed}}}\right)^{\alpha_{\text{B}}}\left(\frac{t}{t_{\text{Sed}}}\right)^{-\frac{\alpha+1}{2}} & t_{\text{B}} \leq t \end{cases} , \quad (5)$$

where the maximum energy, limited by cooling during the free expansion phase, is given by

$$E_{\text{m,S}} = 9m_e^2c^{5/2}(R_{\text{sh}}(t_{\text{Sed}}))^2/(8\eta_{\text{g,free}}\eta_{\text{acc}}ct_{\text{Sed}}^{3/2}E_{\text{knee}}^{1/2}),$$

where  $\eta_{\text{g,free}} \approx 1$  is a gyrofactor during the free expansion phase and  $E_{\text{knee}} = 10^{15.5}$  eV is the knee energy. In accordance with Ohira et al. (2012), the maximum energy of accelerated electrons is given by

$$E_{\text{e,m}} = \min(E_{\text{m,age}}, E_{\text{m,cool}}, E_{\text{m,esc}}) . \quad (6)$$

Correspondingly, the maximum energy of accelerated protons is represented by

$$E_{\text{p,m}} = E_{\text{knee}} \times \begin{cases} \left(\frac{t}{t_{\text{Sed}}}\right) & (t \leq t_{\text{Sed}}) \\ \left(\frac{t}{t_{\text{Sed}}}\right)^{-\alpha} & (t_{\text{Sed}} \leq t) \end{cases} . \quad (7)$$

In Figure 1, we present the evolution of the SNR's radius, its shock velocity, the electron and proton cut-off energies, and the magnetic field (see Sect. 2.2 for details). At the early stages, the results show that the maximum energies of electrons and protons are limited by the SNR's age. Later, the maximum energy of electrons is limited by significant synchrotron cooling, and the escape time when the acceleration time of the diffusive shock acceleration is equal to the escape time due to diffusion. Cooling is not important in limiting the maximum energy for a proton.

Considering the change of the magnetic field in the SNR, the upstream magnetic field is expressed by (Ohira et al. 2012)

$$B(t) = \begin{cases} B_{\text{free}} & t \leq t_{\text{Sed}} \\ B_{\text{free}}\left(\frac{t}{t_{\text{Sed}}}\right)^{-\alpha_{\text{B}}} & t_{\text{Sed}} \leq t \leq t_{\text{B}} \\ B_{\text{ISM}} & t_{\text{B}} \leq t \end{cases} , \quad (8)$$

where the amplified magnetic field during the free expansion phase is

$$B_{\text{free}} = \eta_{\text{g,free}}\eta_{\text{acc}}ct_{\text{Sed}}E_{\text{knee}}/(3eR_{\text{S}}^2).$$

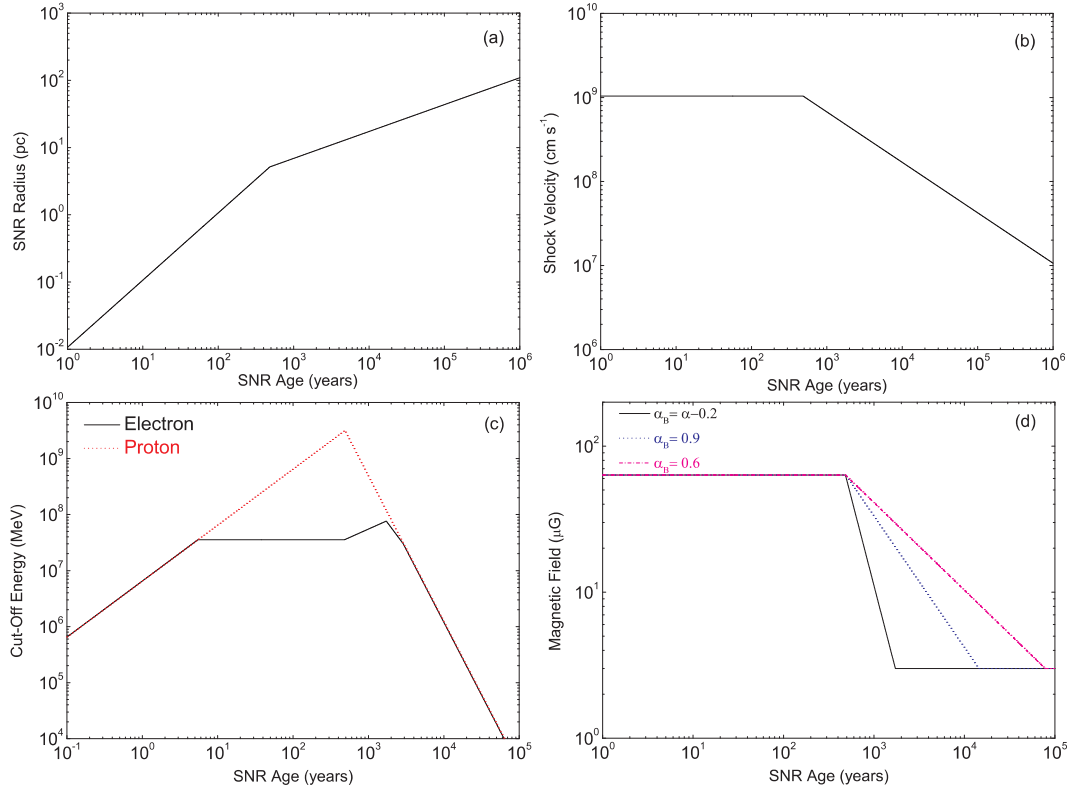


**Fig. 1** The evolution of the SNR's radius, its shock velocity, the electron and proton cutoff energies, and the magnetic field versus the age of the SNR for  $M_{\text{ej}} = 1.4 M_{\odot}$ ,  $v_0 = 10^9 \text{ cm s}^{-1}$ , and  $n_{\text{ISM}} = 0.1 \text{ cm}^{-3}$ .

The gyrofactor is given by

$$\eta_{\text{g}}(t) = \eta_{\text{g,free}} \times \begin{cases} 1 & t \leq t_{\text{Sed}} \\ \left(\frac{t}{t_{\text{Sed}}}\right)^{\alpha - \alpha_{\text{B}} - \frac{1}{5}} & t_{\text{Sed}} \leq t \leq t_{\text{B}} \\ \left(\frac{t_{\text{B}}}{t_{\text{Sed}}}\right)^{-\alpha_{\text{B}}} \left(\frac{t}{t_{\text{Sed}}}\right)^{\alpha - \frac{1}{5}} & t_{\text{Rad}} \leq t \end{cases}, \quad (9)$$

in which the time for the magnetic field amplification to end is  $t_{\text{B}} = t_{\text{Sed}}(B_{\text{free}}/B_{\text{ISM}})^{(1/\alpha_{\text{B}})}$ , with the three evolutions of the magnetic field for  $t_{\text{S}} < t < t_{\text{B}}$  (Bell 2004; Völk et al. 2005; Vink 2008), namely,  $\alpha_{\text{B}}$  is equal to  $\alpha - 0.2$  for  $\eta_{\text{g}} = \eta_{\text{g,free}}$ ,  $0.9$  for  $B^2 \propto u_{\text{sh}}^3$ , and  $0.6$  for  $B^2 \propto u_{\text{sh}}^2$ , respectively. After the time that the amplification of the magnetic field ends,  $t_{\text{B}}$ ,  $B(t)$  is equal to the strength of the magnetic field in the interstellar medium  $B_{\text{ISM}}$  for  $t \geq t_{\text{B}}$ . Here  $B_{\text{ISM}} = 3 \mu\text{G}$  and  $\alpha = 2.6$  are assumed. The predicted value of the magnetic field in the downstream region  $B_{\text{d}}(t) = 4B(t)$  takes the shock compression into consideration.

In Figure 1, the three evolutions of the upstream magnetic field are shown. We find that the magnetic field amplification is significant for young SNRs, and the evolution is consistent for three cases at the early age. In this paper we adopt the first case  $\alpha - 0.2$ . For old SNRs, the magnetic field is usually small, and its value is close to  $B_{\text{ISM}}$  at the end of the evolution.

## 2.2 Particle Energy Distributions and Photon Emission

The energy spectrum of the accelerated particles can be obtained by solving the time-dependent kinetic equation (Malkov & O’C Drury 2001). The volume-averaged production rates of the shock-accelerated electrons and protons are given by (Sturmer et al. 1997)

$$Q_i^{\text{pri}}(E_i, t) = Q_i^0 G(t) \left[ E_i (E_i + 2m_i c^2) \right]^{-[(\beta+1)/2]} (E_i + m_i c^2) \exp(-E_i/E_{i,m}(t)), \quad (10)$$

where  $i = e, p$ ,  $G(t) = R_{\text{sh}}(t_{\text{Sed}})/R_{\text{sh}}(t)$  for  $t \leq t_{\text{rad}}$  and  $G(t) = 0$  for  $t > t_{\text{rad}}$ , and  $\beta$  is the spectral index;  $E_{e,m}$  and  $E_{p,m}$  have been presented in Section 2.1.  $Q_e^0$  and  $Q_p^0$  are used to normalize the particle spectra, and  $E_{\text{par}} = \eta M_{\text{ej}} v_0^2 / 2$  is the total amount of kinetic energy contained in both the injected electrons and the injected protons, where  $\eta \sim 0.1$  presents the efficiency of the kinetic energy of the ejecta being converted into the kinetic energy of both the electrons and the protons.  $K_{\text{ep}} = Q_e^0/Q_p^0$  is a parameter used in the calculation of  $Q_e^0$  and  $Q_p^0$ .

Caprioli et al. (2010) have shown that the accelerated particles at the shock reach their maximum energy near the Sedov stage, therefore it is possible that both the electrons and protons obtain their highest kinetic energies more or less during the Sedov stage. On this basis, the multiband emission spectra of four middle-aged SNRs have been given by Tang et al. (2011a), and most importantly of all, the results of the model were consistent with observed data from the Fermi spacecraft. In addition, Tang et al. (2011b) investigated the radiation spectrum of the young Tycho’s SNR. The results showed that the total amount of kinetic energy contained in the injected particles has been completely converted into the kinetic energy of both electrons and protons from the earlier stage. Here we define the parameter  $t_{\text{ci}} = T$  ( $T > t_{\text{Sed}}$ ), that is to say, the acceleration of particles is dominant during the time  $t_{\text{ci}}$ , hence

$$E_{\text{par}} = \int_0^{t_{\text{ci}}} dt V(t) \left[ \int_0^{E_{e,m}} dE E Q_e(E, t) + \int_0^{E_{p,m}} dE E Q_p(E, t) \right], \quad (11)$$

in which  $V(t) = 4\pi R_{\text{SNR}}^3(t)/3$ , and the maximum energies  $E_{e,m}$  and  $E_{p,m}$  are calculated in Section 2.1. Obviously, for young SNRs, the conversion speed of the kinetic energy contained in the injected particles seems to be quicker than for the middle-aged SNR.

In the interior of the SNR, with the assumptions of a constant density  $n_{\text{SNR}} = 4n_{\text{ISM}}$ , corresponding to the volume of the shell representing the SNR  $V_{\text{Shell}}(t) = V(t)/4$ , the differential densities of accelerated electrons and protons  $n_e(E_e, t)$  and  $n_p(E_p, t)$  are obtained by solving the Fokker-Planck equations in energy space, exactly as in (Zhang & Fang 2007)

$$\begin{aligned} \frac{\partial n_i(E_i, t)}{\partial t} = & -\frac{\partial}{\partial E_i} \left[ \dot{E}_i^{\text{tot}} n_i(E_i, t) \right] + \frac{1}{2} \frac{\partial^2}{\partial E_i^2} [D(E_i, t) n_i(E_i, t)] \\ & + Q_i(E_i, t) - \frac{n_i(E_i, t)}{\tau_i}, \end{aligned} \quad (12)$$

in which  $i = e, p$ , and the terms on the right-hand side of Equation (12) represent systematic energy losses, diffusion in energy space, the particle source function and catastrophic energy loss. Zhang & Fang (2007) gave the details of the calculation process.

In the model, the direction- and volume-averaged electron and proton intensities at each moment during the SNR lifetime can be calculated by the following expressions:  $J_e(E_e, t) = (c\beta/4\pi)n_e(E_e, t)$  and  $J_p(E_p, t) = (c\beta/4\pi)n_p(E_p, t)$ . Subsequently, we calculate non-thermal photon spectra by using the accelerated electron and proton intensities with a single power-law particle injection (Sturmer et al. 1997). For electrons and positrons, the photon emission from the SNR can be reproduced by synchrotron radiation, bremsstrahlung, and inverse Compton scattering. However, for protons, gamma-rays produced by the neutral  $\pi^0$  decay in the proton-proton interaction significantly

contribute to the non-thermal radiation of the SNR; the formulae for all of these radiation processes have been presented in detail in Zhang & Fang (2007). The main inputs of the model include the age  $T$  and the distance  $d$  from the source, initial ejecta mass  $M_{\text{ej}}$ , initial explosion energy  $E_{\text{SN}}$ , conversion efficiency  $\eta$ , electron-to-proton ratio  $K_{\text{ep}}$ , spectral index  $\alpha$ , and hydrogen density  $n_{\text{ISM}}$ .

### 3 APPLICATIONS

In this section, we apply the model to two young SNRs: SN 1006 (G327.6+14.6) and Kepler's SNR (G4.5+6.8). The comparisons of our modeling results with the observed data are shown in Figures 2 and 3. In the two figures, the non-thermal photon spectra are indicated as the dashed, dot-dashed, dotted, and dash-dot-dotted lines, which represent the spectra through synchrotron emission, inverse Compton scattering, bremsstrahlung, and the spectra from the  $\pi^0$ -decay process, respectively.

The source of SN 1006 was recorded by Chinese and Arab astronomers on 1006 May 1 (Stephenson & Green 2002), so its present age is 1005 yr. It is an ideal example of a shell-type SNR, because of the evolution in its luminosity. Schaefer (1996) demonstrated that it is the result of a type Ia supernova explosion, and they thought that it was probably the brightest supernova in recorded history. Based on comparing the optical proper motion with an estimate of the shock velocity, Winkler et al. (2003) derived a distance of 2.2 kpc for this SNR. We make a simple assumption that the ejected material has been exploding into a uniform medium and magnetic field after the supernova explosion. In view of the upper end of the typical range of type Ia SN explosion energies (Woosley et al. 2007), we assume that the initial explosion energy is equal to  $1.3 \times 10^{51}$  erg for SN 1006. Katsuda et al. (2009) have pointed out that the surrounding gas density is rather low for this source,  $n_{\text{ISM}} = 0.085 \text{ cm}^{-3}$ . The remnant of SN 1006 was first identified in radio (Gardner & Milne 1965), with Reynolds & Chevalier (1982) describing the first radio images of the SNR. The observations with the ASCA and ROSAT have confirmed a non-thermal component of hard X-rays from SN 1006 (Koyama et al. 1995; Willingale et al. 1996), then a small-scale structure in the nonthermal X-ray filaments of SN 1006 was presented by the detection of Chandra (Bamba et al. 2003; Long et al. 2003). Rothenflug et al. (2004) also showed evidence of the X-ray observations of XMM-Newton, and the radio emission was confirmed to be related to nonthermal X-rays. Deep observations at VHE energies (above 100 GeV) were made with the HESS array of Cherenkov Telescopes (Acero et al. 2010), and their results indicated that the bipolar morphology in the  $\gamma$ -ray band was also consistent with the observations in the X-ray band, which support a major result of the diffusive shock acceleration theory.

We model the multiband emission of SN 1006 with a simple time-dependent injection model; some parameters involved in the model are shown in Table 1. As shown in Figure 2, it is obvious that the radio emission is from synchrotron emission generated by accelerated electrons, which is extended up to the X-rays in accordance with the detection of SN 1006 (Rothenflug et al. 2004). The value of spectral index  $\alpha$  is equal to 2.1 in this model (Petruk et al. 2011). The high energy gamma-rays are probably from the inverse Compton scattering, bremsstrahlung and p-p interaction; here the soft photons of inverse Compton scattering are from Cosmic Microwave Background (CMB) emission. The results show that the inverse Compton scattering and the proton-proton interaction dominated the VHE gamma-ray emission, but the contribution of the bremsstrahlung seems to be negligible for the source. In our calculation,  $K_{\text{ep}} = 0.0035$ , which is approximately consistent with the cosmic ray composition observed at the Earth (Abdo et al. 2010). In consideration of the evolution of the magnetic field, the magnetic field in the shocked downstream region  $B_d \simeq 45 \mu\text{G}$  is calculated by Equation (8) at the current epoch (i.e.,  $t = T$ ).

Kepler's SNR exploded in 1604. Baade (1943) initially considered it to be a type Ia by studying the historical light curve of the SNR, however this is a controversial issue. Up to now, some observational evidence has favored the result of a type Ia supernova explosion, such as the thermal X-ray spectra obtained with ASCA (Kinugasa & Tsunemi 1999), Chandra (Hwang et al. 2000) and

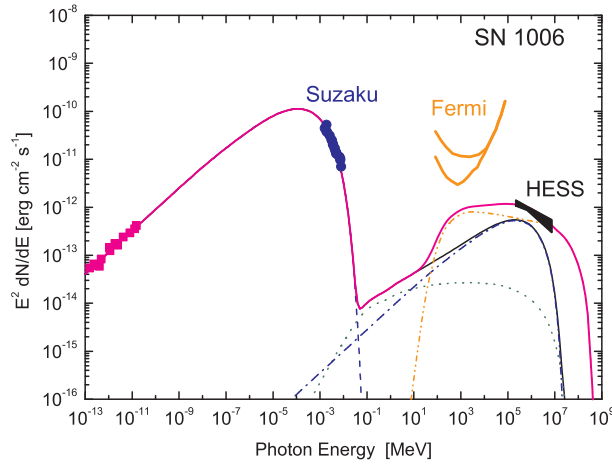


**Fig. 2** Multiband emission spectra of SN 1006. The radio (from Reynolds 1996) and X-ray emissions (Bamba et al. 2008) are explained by synchrotron radiation from relativistic electrons, while the gamma-ray emission (Acero et al. 2010) is from the sum of bremsstrahlung (*dotted line*), inverse Compton scattering (*dot-dashed line*) and  $\pi^0$ -decay (*dash-dot-dotted line*). The Fermi LAT sensitivity for one year is shown (*concave line*) for the Galactic (*upper*) and extragalactic (*lower*) background (Acero et al. 2010). Details of the model are described in the text.

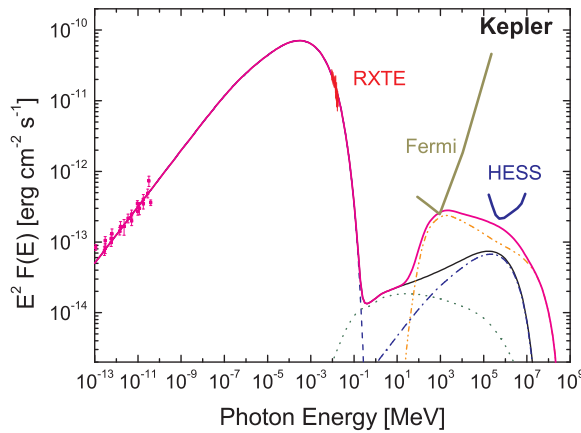


**Fig. 3** Multiband emission spectra from Kepler's SNR. All of the curves denote the same as in the caption of Fig. 2. The physical parameters are shown in Table 1. The radio data (Reynolds & Ellison 1992) and X-ray data (Allen 1999) for the entire SNR are indicated, and the respective sensitivities of Fermi over one year and of HESS are from Berezhko et al. (2007). Details of the models are described in the text.

XMM-Newton (Cassam-Chenaï et al. 2004); this was confirmed by corresponding theoretical analysis (Bamba et al. 2005; Reynolds et al. 2007). Based on the so-called delayed-detonation model of a type Ia supernova explosion, Gamezo et al. (2005) deduced a typical range of explosion energy  $E_{\text{SN}} = (1.3 - 1.6) \times 10^{51}$  erg, however a lower energy  $E_{\text{SN}} = (0.4 - 0.6) \times 10^{51}$  erg was given with the deflagration model (Reinecke et al. 2002). The distance of Kepler's SNR is also uncertain.

**Table 1** Model Parameters in Our Calculations. In the model, we assume the same values of the initial mass  $M_{\text{ej}}$  and conversion factor  $\eta$  for the two SNRs:  $M_{\text{ej}} = 1.3 M_{\odot}$  and  $\eta = 0.1$ .

Model Parameter	SN 1006	Kepler's SNR
Age $T$ (yr)	1005	400
Distance $d$ (kpc)	2.2	7.0
Initial explosion energy $E_{\text{SN}}$ ( $10^{51}$ erg)	1.3	1.0
ISM hydrogen density $n_{\text{ISM}}$ ( $\text{cm}^{-3}$ )	0.085	0.2
Electron/positron ratio $K_{\text{ep}}$	0.0035	0.007
Spectral index $\alpha$	2.1	2.2

Reynoso & Goss (1999) derived a lower limit of  $(4.8 - 1.4)$  kpc and an upper limit of 6.4 kpc. Chiotellis et al. (2012) suggested a distance of  $\geq 6$  kpc, in agreement with the result of Aharonian et al. (2008). Berezhko et al. (2007) provided a range of distances  $d = 3.4 - 7$  kpc. In view of the above analysis, in this paper we fit the values at  $E_{\text{SN}} = 10^{51}$  erg and  $d = 7$  kpc. In the radio band, Dickel et al. (1988) studied the significantly decelerating expansion of this SNR. The data on radio emission for Kepler's SNR can be found in Reynolds & Ellison (1992). The X-ray data from Kepler's SNR have been given by Allen (1999). Berezhko et al. (2007) expected the flux of gamma-ray emission for this SNR to be at TeV energy, and the respective sensitivities with Fermi LAT over one year and with HESS were shown in their work.

The multiband emission spectra of Kepler's SNR is presented in Figure 3. Here one choice is to assume that the age  $T = 400$  yr and  $n_{\text{ISM}} = 0.2 \text{ cm}^{-3}$ . The differential spectral index of about 2.2 was implied by the radio-to-X-ray synchrotron spectra (Allen et al. 1999). Similar to SN 1006 (a type Ia supernova explosion), the ejected mass  $M_{\text{ej}} = 1.3 M_{\odot}$  is used in the model. The above-mentioned numerical factor  $\eta_{\text{acc}}$  is equal to 4.5 for modeling the spectra of Kepler's SNR. The results show that the radio-to-X-ray emission is explained well by the synchrotron emission from relativistic electrons. The gamma-ray emission is mainly from inverse Compton scattering of the CMB photons and  $\pi^0$  decay due to the relativistic protons colliding with the ambient medium. Here the bremsstrahlung is also negligible. In the model, when time  $t = T$ , the magnetic field in the shock downstream  $B_{\text{d}} \simeq 105 \mu\text{G}$  is produced by Equation (8), making the amplification effect of the magnetic field more obvious than in the result from SN 1006.

#### 4 SUMMARY AND DISCUSSION

In this paper, we revisit the dynamic evolution of the SNR, then the maximum energies of the accelerated electrons and protons are given. The evolution of the magnetic field is cast in a time-dependent model for reproducing the multiband photon emissions. Here we assume that the total amount of kinetic energy contained in the injected particles has been completely converted into kinetic energy of both the electrons and protons during time  $t_{\text{ci}} = T$  (here  $T > t_{\text{sed}}$ ). The results show that the non-thermal photon spectra have a peak at the radio-to-X-ray band, and these photons are from electron synchrotron emission. Another peak is at gamma-ray energies. The gamma-rays are probably produced by the inverse Compton scattering, bremsstrahlung and  $\pi^0$  decay due to the relativistic protons colliding with the ambient medium. We have applied this model to two young SNRs with reasonable model parameters. The cosmic-ray composition observed at the Earth suggested  $K_{\text{ep}} \sim 0.01$ , but in our calculation, 0.007 and 0.0035 were respectively adopted for Kepler's SNR and SN 1006. This is also reasonable for the selection of the parameters, as described in the above sections. Although we can explain the observations from radio to TeV gamma-rays for the two young SNRs, we cannot distinguish either the leptonic origin or hadronic origin by only comparing the model results with the observed gamma-ray data.

For SNR SN 1006, with radio and X-ray data integrated over the full remnant, Acero et al. (2010) modeled the spectral energy distribution of the source by using a simple one-zone stationary model. The distribution of particles is prescribed with a given power-law spectrum with an exponential cutoff. Using different parameters, they reproduced the broadband spectra of SN 1006 with a leptonic scenario, a hadronic one and a mixed leptonic/hadronic scenario. The spectral index is fitted at 2.1 except for the hadronic scenario (the value is 2.0); a total explosion energy  $E_{\text{SN}}$  and the electron-to-proton ratio  $K_{\text{ep}}$  are also different for each case. The magnetic field amounts to 120  $\mu\text{G}$  and 45  $\mu\text{G}$  for the other two cases, respectively. This is the result in Acero et al. (2010). Petruk et al. (2011) put forward some observational constraints on the kinetic energy and magnetic field, including modeling and a comparison of observed characteristics for SN 1006. They found that the magnetic field strength  $B$  in the shock's upstream region could be equal to 12  $\mu\text{G}$  if the spectral index  $\alpha = 2.1$ , and  $B = 25 \mu\text{G}$  if  $\alpha = 2.0$ . In our paper, the magnetic field strength  $B_{\text{d}} \simeq 45 \mu\text{G}$ , i.e., here  $B = 11.25 \mu\text{G}$ . This value is approximately in agreement with  $B = 12 \mu\text{G}$ . For Kepler's SNR, with a typical explosion energy  $E_{\text{SN}} = 10^{51}$  erg, Berezhko et al. (2007) predicted the energy flux of TeV gamma-rays to vary from  $2 \times 10^{-11}$  to  $10^{-13}$  erg  $\text{cm}^{-2} \text{s}^{-1}$  when the distance changes from 3.4 to 7 kpc. Using the nonlinear kinetic theory of cosmic ray acceleration in SNRs, they found that the gamma-ray emission is dominated by  $\pi^0$ -decay due to relativistic protons colliding with the ambient medium; an interior magnetic field strength  $B_{\text{d}} = 480 \mu\text{G}$  was used for a good fit. In addition, Völk et al. (2005) gave the value of  $B_{\text{d}} = 250 \mu\text{G}$  through the observed spatial fine structure of the synchrotron emission. In our calculations, the magnetic field strength  $B_{\text{d}} \simeq 105 \mu\text{G}$  is lower than those values derived from their methods. The distance of Kepler's SNR is not known very well, as stated in Berezhko et al. (2007). If the actual source distance is larger than 7 kpc, it is difficult to detect gamma-rays. We fit a distance of  $d = 7$  kpc because there has been no observation in gamma-rays up to now.

To sum up, the radio-to-X-ray spectra from SN 1006 and Kepler's SNR can be explained by the synchrotron emission from relativistic electrons, in which the magnetic field amplification is of great importance. Although VHE gamma-rays from SN 1006 were detected firstly by the HESS collaboration, it is still uncertain that the gamma-rays have a leptonic or hadronic genesis. Measurements in the GeV-energy range would be important to distinguish between the different origins. Unfortunately, the gamma-rays from Kepler's SNR have not been observed up to now, thus we are looking forward to the detection of the gamma-rays from it, which are also vital in limiting the distance to this SNR.

**Acknowledgements** This work is partially supported by the National Natural Science Foundation of China (Grant No. 11173020) and the National Basic Research Program of China (973 Program, 2009CB824800).

## References

- Abdo, A. A., Ackermann, M., Ajello, M., et al. 2010, *Science*, 327, 1103  
 Acero, F., Aharonian, F., Akhperjanian, A. G., et al. 2010, *A&A*, 516, A62  
 Aharonian, F., Akhperjanian, A. G., Barres de Almeida, U., et al. 2008, *A&A*, 488, 219  
 Allen, G. 1999, in *International Cosmic Ray Conference*, 3, 480  
 Baade, W. 1943, *ApJ*, 97, 119  
 Bamba, A., Yamazaki, R., Ueno, M., & Koyama, K. 2003, *ApJ*, 589, 827  
 Bamba, A., Yamazaki, R., Yoshida, T., Terasawa, T., & Koyama, K. 2005, *ApJ*, 621, 793  
 Bamba, A., Fukazawa, Y., Hiraga, J. S., et al. 2008, *PASJ*, 60, 153  
 Becker, R. H., White, N. E., Boldt, E. A., Holt, S. S., & Serlemitsos, P. J. 1980, *ApJ*, 237, L77  
 Bell, A. R. 1978, *MNRAS*, 182, 147  
 Bell, A. R. 2004, *MNRAS*, 353, 550  
 Berezhko, E. G., Ksenofontov, L. T., & Völk, H. J. 2007, *Ap&SS*, 309, 385

- Berezhko, E. G., Ksenofontov, L. T., & Völk, H. J. 2009, *A&A*, 505, 169
- Blandford, R. D., & Ostriker, J. P. 1978, *ApJ*, 221, L29
- Caprioli, D., Amato, E., & Blasi, P. 2010, *Astroparticle Physics*, 33, 160
- Cassam-Chenaï, G., Decourchelle, A., Ballet, J., et al. 2004, *A&A*, 414, 545
- Chiotellis, A., Schure, K. M., & Vink, J. 2012, *A&A*, 537, A139
- Dickel, J. R., Sault, R., Arendt, R. G., Korista, K. T., & Matsui, Y. 1988, *ApJ*, 330, 254
- Gamezo, V. N., Khokhlov, A. M., & Oran, E. S. 2005, *ApJ*, 623, 337
- Gardner, F. F., & Milne, D. K. 1965, *AJ*, 70, 754
- Hwang, U., Holt, S. S., Petre, R., Szymkowiak, A. E., & Borkowski, K. J. 2000, in *AAS/High Energy Astrophysics Division #5, Bulletin of the American Astronomical Society*, 32, 1236
- Katsuda, S., Petre, R., Long, K. S., et al. 2009, *ApJ*, 692, L105
- Kinugasa, K., & Tsunemi, H. 1999, *PASJ*, 51, 239
- Koyama, K., Petre, R., Gotthelf, E. V., et al. 1995, *Nature*, 378, 255
- Long, K. S., Reynolds, S. P., Raymond, J. C., et al. 2003, *ApJ*, 586, L1162
- Lozinskaya, T. A. 1992, *Supernovae and Stellar Wind in the Interstellar Medium* (New York: AIP)
- Malkov, M. A., & O’C Drury, L. 2001, *Reports on Progress in Physics*, 64, 429
- Ohira, Y., Yamazaki, R., Kawanaka, N., & Ioka, K. 2012, *MNRAS*, 427, 91
- Petruk, O., Beshley, V., Bocchino, F., Miceli, M., & Orlando, S. 2011, *MNRAS*, 413, 1643
- Reinecke, M., Hillebrandt, W., & Niemeyer, J. C. 2002, *A&A*, 386, 936
- Reynolds, S. P., & Chevalier, R. A. 1982, in *Bulletin of the American Astronomical Society*, 14, 936
- Reynolds, S. P., & Ellison, D. C. 1992, *ApJ*, 399, L75
- Reynolds, S. P. 1996, *ApJ*, 459, L13
- Reynolds, S. P., Borkowski, K. J., Hwang, U., et al. 2007, *ApJ*, 668, L135
- Reynoso, E. M., & Goss, W. M. 1999, *AJ*, 118, 926
- Rothenflug, R., Ballet, J., Dubner, G., et al. 2004, *A&A*, 425, 121
- Schaefer, B. E. 1996, *ApJ*, 459, 438
- Stephenson, F. R., & Green, D. A. 2002, *Historical Supernovae and Their Remnants*, eds. F. Richard Stephenson and David A. Green, *International Series in Astronomy and Astrophysics 5* (Oxford: Clarendon Press)
- Sturmer, S. J., Skibo, J. G., Dermer, C. D., & Mattox, J. R. 1997, *ApJ*, 490, 619
- Tang, Y. Y., Fang, J., & Zhang, L. 2011a, *ApJ*, 739, 11
- Tang, Y.-Y., Fang, J., & Zhang, L. 2011b, *Chinese Physics Letters*, 28, 109501
- Vink, J. 2008, in *American Institute of Physics Conference Series*, 1085, eds. F. A. Aharonian, W. Hofmann, & F. Rieger, 169
- Völk, H. J., Berezhko, E. G., & Ksenofontov, L. T. 2005, *A&A*, 433, 229
- Willingale, R., West, R. G., Pye, J. P., & Stewart, G. C. 1996, *MNRAS*, 278, 749
- Winkler, P. F., Gupta, G., & Long, K. S. 2003, *ApJ*, 585, 324
- Woodsley, S. E., Kasen, D., Blinnikov, S., & Sorokina, E. 2007, *ApJ*, 662, 487
- Zhang, L., & Fang, J. 2007, *ApJ*, 666, 247